ADVANCES IN ATMOSPHERIC SCIENCES, VOL. 32, DECEMBER 2015, 1592–1602

Ten-Year Climatological Features and Air Origin of Midlatitude Double Tropopauses

WU Xue and LÜ Daren*

Key Laboratory for Atmosphere and Global Environment Observation, Institute of Atmospheric Physics, Chinese Academy of Sciences, Beijing 100029

(Received 2 February 2015; revised 9 May 2015; accepted 28 May 2015)

ABSTRACT

The 10-year climatological features related to midlatitude double tropopause events (DTs) are examined using ERA-Interim data from 2003 to 2012. The analysis is based on tropopauses defined by lapse rate. Results show that DTs are permanent or semi-permanent in the midlatitudes, and high DT frequency bands move poleward in winter and equatorward in summer, which is consistent with the seasonal movement of the subtropical jet. Based on our statistics, the second tropopause is found at about 100 hPa in the subtropics and at slightly lower altitudes in sub-polar regions. The thickness between the first and second tropopause is smaller in the subtropics and increases with latitude. Next, the origin of air sandwiched between the first and second tropopause of DTs is studied with a revised version of the UK Universities Global Atmospheric Modelling Programme Offline Trajectory Code (Version 3) diabatic trajectory model. The results show that, in the lower or middle troposphere, air is transported into the DTs from lower latitudes, mainly in the tropics. The dominant source regions are mainly areas of deep convection and steep orography, e.g., the western Pacific and Himalayan Mountains, and they show strong seasonality following the seasonal shift of these strong upwelling regions.

Key words: double tropopause, trajectory model, stratosphere–troposphere exchange

Citation: Wu, X., and D. R. Lü, 2015: Ten-year climatological features and air origin of midlatitude double tropopauses. *Adv. Atmos. Sci.*, **32**(12), 1592–1602, doi: 10.1007/s00376-015-5036-4.

1. Introduction

The tropopause is a boundary that separates the statically unstable troposphere and much more stable stratosphere, and is a transition layer between radiative–convective balance in the troposphere and radiative balance in the stratosphere (Thuburn and Craig, 2002). Two-way transport processes across the tropopause are an important mechanism that influences chemical composition in the upper troposphere and lower stratosphere. However, in the extratropical region especially, the lapse rate–based WMO (1957) definition of the tropopause produces more than one tropopause.

Double tropopauses (DTs), or even triple tropopauses, have been a focus of scientific interest for decades (e.g., Yamanaka, 1992; Yamanaka et al., 1996; Schmidt et al., 2006; Añel et al., 2007; Castanheira et al., 2012). Links between midlatitude DTs and baroclinic waves have been studied using idealized model and GPS radio occultation data, revealing that the location of DTs is associated with baroclinic Rossby wave breaking in the subtropical upper troposphere and lower stratosphere (McIntyre and Palmer, 1983; Lamarque and Hess, 1994; Newman and Schoeberl, 1995; Vaughan and Timmis, 1998; Pan et al., 2009; Castanheira et al., 2012). Moreover, DT structures are considered to be responsible for tropical tropospheric air intruding into the stratosphere above the subtropical jet core (Randel et al., 2007; Pan et al., 2009, 2010). Subsequent studies have shown that the DT structure consists of tropospheric air (low in ozone concentration and static stability) overlapping stratospheric air (high in ozone and static stability), using modelling results and satellite remote sensing data from Aura/HIRDLS and ozonesonde profiles (Olsen et al., 2008; Pan et al., 2009; Homeyer et al., 2011; Vogel et al., 2011), and that DTs are believed to favor cross-tropopause exchange in the subtropics (Sprenger et al., 2003; Bracci et al., 2012).

Recent studies using reanalysis data, GPS radio occultation, radiosonde profiles and satellite data show that DTs are prevalent in the midlatitudes of both hemispheres in all seasons, and the maximum occurrence is during late winter and early spring (Schmidt et al., 2006; Randel et al., 2007; Añel et al., 2008; Castanheira and Gimeno, 2011; Peevey et al., 2012). This may indicate, at least from the perspective of Rossby wave breaking, that there is more subtropical cross-tropopause transport during DTs' maximum occurrence seasons (Horinouchi and Boville, 2000; Waugh and Polvani, 2000). However, even though the above studies have shown that Rossby wave breaking and poleward transport are re-

* Corresponding author: LÜ Daren
Email: ludr@mail.iap.cas.cn

© Institute of Atmospheric Physics/Chinese Academy of Sciences, and Science Press and Springer-Verlag Berlin Heidelberg 2015

sponsible for a significant fraction of DT events, DTs are also frequently found without the presence of Rossby wave breaking (e.g., Biondi et al., 2011) and frequent DT occurrence years are not necessarily years of frequent irreversible mixing events (Olsen et al., 2010). Also, Lagrangian trajectory–based studies show that cross-tropopause transport in the subtropics is more vigorous in summer than in winter (Berthet et al., 2007; Skerlak et al., 2013). This controversy about the seasonal variation of stratosphere–troposphere transport raises the question: what role do DTs play in troposphere-to-stratosphere transport? Peevey et al. (2014) stated that there is a robust global relationship between the DT and the tropical inversion layer through the warm conveyer belt, where the DT frequency increases (decreases) in the extratropics (tropics) as the tropical inversion layer increases in strength. But these systems all have opposing seasonal characteristics and formation mechanisms, demonstrating that the DT is more complicated than previous poleward-transport studies might suggest.

Information on the climatological characteristics of DTs and the origin of air sandwiched within DTs is crucial for qualitative estimates of cross-tropopause exchange. However, there are still different opinions about the origin of air between two tropopauses. Wang and Polvani (2011) suggest that, as shown by an idealized model, air inside the DT structure originates from high latitudes, which is the opposite to some other results (Pan et al., 2009; Añel et al., 2012). This apparent controversy might be caused by different formation mechanisms of midlatitude DT events, e.g., baroclinic wave breaking and synoptic events like cut-off lows (Peevey et al., 2014).

In the present study, we begin by examining the features of midlatitude DT events using ERA-Interim reanalysis data from 2003 to 2012, showing a 10-year climatological spatial distribution of DTs and seasonal variations. Then, the origin of air in DTs is analyzed based on the results of a diabatic Lagrangian trajectory model. In section 2, the input data and trajectory model are described. The results are presented in sections 3 and 4, and discussed in section 5. A summary is given in section 6.

2. Data and methodology

2.1. *ERA-Interim data and analysis*

ERA-Interim is the latest global atmospheric reanalysis results produced by the European Centre for Medium-Range Weather Forecasts (ECMWF) (Simmons et al., 2006; Dee et al., 2011), which covers the period from 1 January 1979 to the present day. Compared with ERA-40, the ERA-Interim forecast model is run at a higher horizontal resolution of T255 (for the full resolution version). In this paper, our analysis of midlatitude DT features employs ERA-Interim data over 10 years from 2003 to 2012 on 60 ECMWF model levels (with a vertical resolution of ~ 1 km in the upper troposphere and lower stratosphere region). These reanalysis temperature data, available daily at four analysis times (0000, 0600, 1200, and 1800 UTC), were utilized to define tropopauses according to the definition from the World Meteorological Organization's Commission for Aerology (WMO, 1957):

(1) The first tropopause is defined as the lowest level at which the lapse rate decreases to 2 K km^{-1} or less, provided also that the average lapse rate between this level and all higher levels within 2 km does not exceed 2 K km^{-1};

(2) If above the first tropopause the average lapse rate between any level and all higher levels within 1 km exceeds 3 K km^{-1}, then a second tropopause is defined by the same criterion as under (a). This tropopause may be either within or above the 1 km layer.

However, due to the relatively low vertical resolution of the ERA-Interim data near tropopauses ($\sim$1 km), a slight modification was made to criterion (b) based on a lapse rate of 2.5 K km^{-1}, to generate a reasonable DT occurrence frequency. A similar approach was employed by Randel et al. (2007) and has been compared with results from GPS radio occultation data to verify its accuracy. Similar methods were also used in other studies when using ECMWF reanalysis data, e.g. Castanheira and Gimeno (2011), Castanheira et al. (2012) and Peevey et al. (2014). The influence of this method on the results is discussed in section 5.

Analysis winds, temperature, and ground pressure are also used to drive the three-dimensional (3D) trajectory model, which is discussed in the following subsection.

2.2. *3D OFFLINE3_diab trajectory model*

To determine the origin of air sandwiched within the DT structure, 3D trajectory integrations are performed using a diabatic trajectory model—OFFLINE3_diab. This is a modification of the third edition of the UK Universities Global Atmospheric Modelling Programme Offline Trajectory Code (Methven, 1997), which is a kinematic trajectory model. Compared with the original kinematic trajectory model, the main difference in the diabatic model is the vertical velocity scheme: vertical (cross-isentropic) velocity is expressed with a diabatic heating rate (a change in potential temperature) instead of being calculated with the horizontal wind through the continuity equation. Diabatic trajectory models show air parcels transported along the isentropic surfaces by large-scale winds and these parcels move across isentropes only by net diabatic heating or cooling. If the heating rate is zero, trajectories move under adiabatic conditions and conserve potential temperature. A comprehensive review of the accuracy of the trajectories calculated using this model is given in Methven (1997) and Stohl (1998). By reducing errors in vertical velocity, diabatic trajectory models can give better results, especially when the models are driven by meteorological fields with low spatial resolutions (Ploeger et al., 2010, 2011).

The OFFLINE3_diab model interpolates 3D gridded winds to the trajectory locations using bilinear interpolation (in time and in the horizontal direction) and cubic Lagrangian interpolation (in the vertical direction), and then the trajectories are integrated backward using a 4th-order Runge–Kutta scheme. The backward trajectories were calculated from 6-

hourly ERA-Interim data. Three-dimensional off-line meteorological data, e.g., wind field and temperature, were interpolated to the trajectory locations and values of meteorological fields, including potential vorticity (PV), surface pressure, pressure, temperature, and potential temperature, were assigned as attributes for the particles at each integration time.

The trajectories were initialized on grid resolutions of $1^\circ \times 1^\circ \times 5$ K (with 17 vertical levels from 340 K to 420 K) covering the whole globe (altogether 556 920 particles), and the initial meteorological data were provided every 6 hours at 0000, 0600, 1200, and 1800 UTC; particles were released every 12 hours and the outputs were provided every 3 hours. The vertical range (from 340 K to 420 K) covers nearly all DT structures and sensitivity experiments on the spatial resolutions specified. Additionally, release intervals of the trajectories showed that the origin of air in DTs is not sensitive to the initial settings of the trajectories. The settings used in this study were proved to be sufficient to generate smooth and robust features and overall physical characteristics.

3. Features of midlatitude DTs

In this section, ERA-Interim data from 2003 to 2012 are used to reveal the spatial distribution and characteristics of DTs.

Figure 1 shows a vertical cross section of a typical DT event. In this case, the spatial extent of a DT event is significant and the structure is clearly outlined. This case is located over the eastern Pacific Ocean and lasts for about 3 days and extends from about 20°N to 50°N. The air between the first and second tropopauses could be divided into two parts by the 2 K km^{-1} isocline. The poleward intrusion contains air with lapse rate higher than 2 K km^{-1}, and low static stability (vertical gradients of potential temperature). The proportional distribution of PV in the poleward intrusion is calculated with ERA-Interim data and is shown in Fig. 1c. It indicates that PV for the majority of air in the poleward intrusion is larger than 4 PVU (1 PVU =10^{-6} K kg^{-1} m^2 s^{-1}), especially in summer (June–July–August, JJA). And if the dynamic tropopause in the midlatitudes is defined by PV values between 2 PVU to 4 PVU, then air with tropospheric characteristics has notably intruded into the stratosphere. The layer below the poleward intrusion, which contains air with lower lapse rate and higher static stability, is more stratospheric in nature.

Figure 2 displays the seasonal geographical distribution of the DT frequency of occurrence in winter (December–January–February, DJF) and summer (JJA), showing the preferred regions of formation and seasonal difference. DTs are permanent or semi- permanent in midlatitudes for both hemispheres. And generally, DT frequencies are maximum (minimum) during the winter (summer) in both hemispheres, which agrees well with previous studies (e.g., Schmidt et al., 2006; Añel et al., 2007; Randel et al., 2007; Castanheira and Gimeno, 2011, Peevey et al., 2012). Moreover, the maximum frequencies of the Northern Hemisphere in DJF are larger

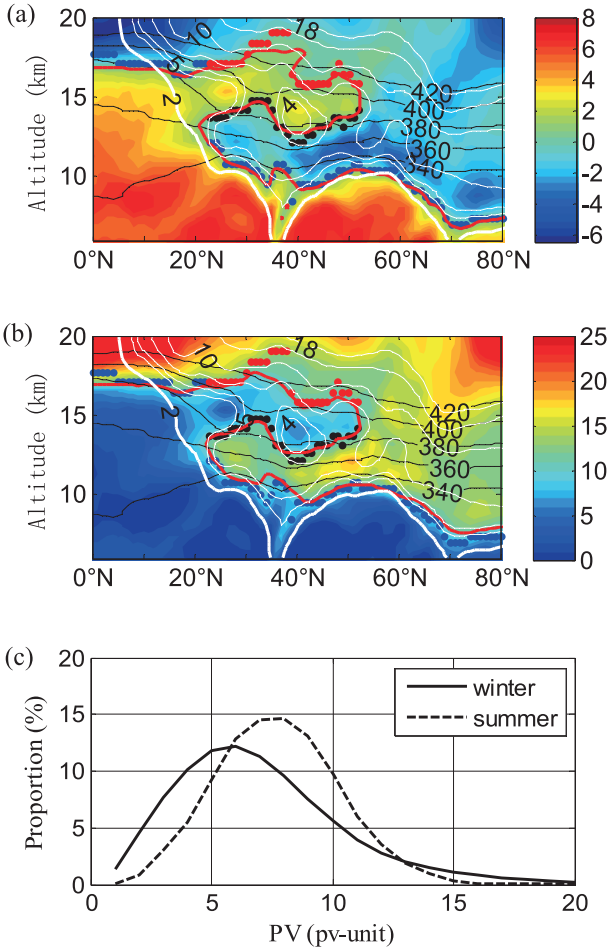

Fig. 1. Cross section, along 238°E at 0800 UTC 26 January 2006, of (a) lapse rate (units: K km^{-1}) and (b) static stability (units: K km^{-1}). Superimposed are the location of the first tropopause (blue dots), the second tropopause (red dots), the location where the search for second tropopauses started (black dots), the 2 K km^{-1} WMO criterion (red contour), potential temperature (black contours), and potential temperature (white contours; 2 PVU contour is highlighted as the thicker white contour). Statistics on the proportion of PV values between red dots and black dots in winter (DJF) and summer (JJA) are shown in (c).

than the maximum frequencies of the Southern Hemisphere in JJA. This may be due to the differences in the homogeneity of the land–sea distribution in the two hemispheres (Schmidt et al., 2006), i.e., extensive mountain ranges may enhance the propagation of planetary waves forced by topography in the Northern Hemisphere (Holton, 2004).

In DJF, DT frequencies between 30°N and 45°N are between 35% and 60%, except for the eastern Pacific and central Atlantic region. Frequencies in the northern Atlantic are relatively high compared to other areas at the same latitudes. In the Southern Hemisphere, maximum DT frequency is about 15%, which is much smaller than that in the Northern Hemisphere. In JJA, frequencies are higher in the Southern Hemisphere, located between 25°S and 45°S, and the maxima appear at the south of Australia and the sea to its east.

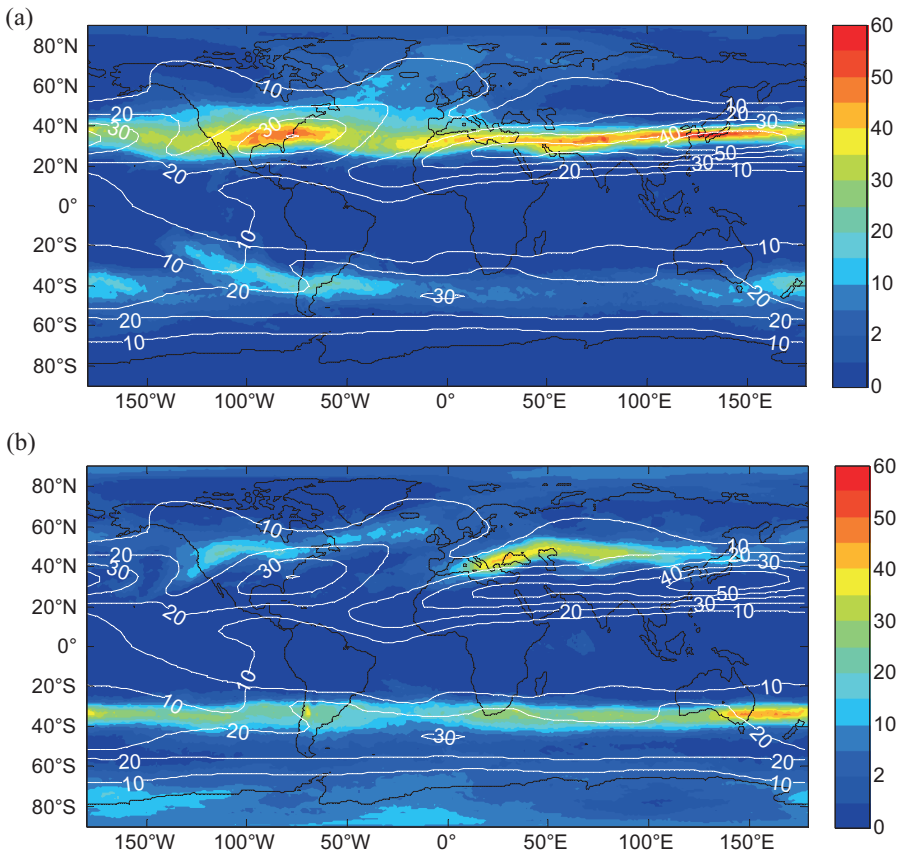

Fig. 2. DT frequency of occurrence (%) obtained using ERA-Interim data. Plots show data from 2003 to 2012 for (a) winter (DJF) and (b) summer (JJA). Superimposed is the seasonal mean zonal wind (white contours) with the following levels: 10, 20, 30, 40 and 50 m s^{-1} on the 200 hPa pressure level.

Notably, there is a band of high DT frequency in the midwest Eurasian continent, ranging from about 40°N to 55°N and the maxima can reach about 35%. And over the Andes Mountains in South America, DT frequency remains relatively high, compared with the rest of the Southern Hemisphere. Some localized maxima of frequencies, such as those over the Tibetan Plateau and the southern part of South America, also observed in some previous studies (Schmidt et al., 2006; Randel et al., 2007; Peevey et al., 2012), may be a result of the summer monsoon circulation (Holton, 2004) or the summer monsoon anticyclone (Randel et al., 2007), and large orography like the Tibetan Plateau and the Andes.

In both hemispheres, high DT frequency bands move poleward in the winter and equatorward in the summer, which is consistent with the seasonal movement of the subtropical jet. As seen in Fig. 3, the second tropopause always appears above and poleward of the subtropical jet core where the baroclinic instability of the subtropical jet exits (Pan and Munchak, 2011; Manney et al., 2014). Maxima of occurrence frequencies are larger and located at higher latitudes in the winter hemisphere.

Based on our statistics, a schematic diagram of midlatitude DTs is drawn in Fig. 4. The first tropopause can reach up to a height higher than 100 hPa in the tropics, and the vertical location of the first tropopause decreases steeply poleward, located between 300 hPa and 200 hPa. DTs are permanent or semi-permanent at midlatitudes, with the second tropopause existing at about 100 hPa in the subtropics and slightly lower in sub-polar regions. The DT thickness, which is defined by the height differences between the first and second tropopause, is smaller in the subtropics and increases with latitude. Air within DTs can be divided into two types. Air in area I is tropospheric, characterized by a high lapse rate and low static stability, as seen in Fig. 1; air in area II is characterized by a low lapse rate and high static stability. High-resolution satellite data also display low ozone concentration for air in area I and there is a large ozone concentration gradient between area I and area II (Pan et al., 2009).

4. Origin of air between DTs

Determining the origin of the air sandwiched within DTs is helpful for estimating the significance of DTs in troposphere-to-stratosphere transport. In this section, air parcels between DTs in the Northern Hemisphere and Southern Hemisphere are tracked separately using backward trajec-

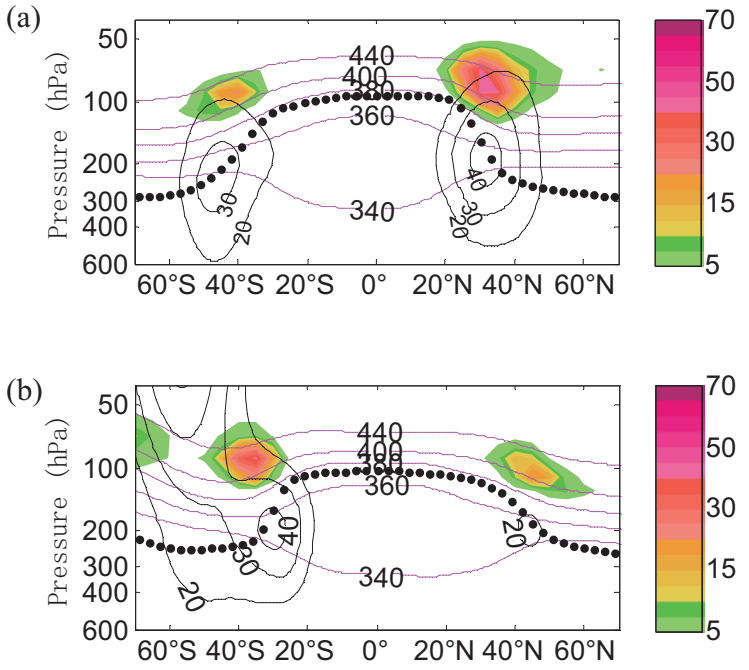

Fig. 3. Zonal mean of second tropopause occurrence (%) for (a) winter (DJF) and (b) summer (JJA). Results are binned every 5° of latitude and every 10 hPa in pressure. Seasonal mean zonal wind (black contours; units: m s^{-1}) is plotted.

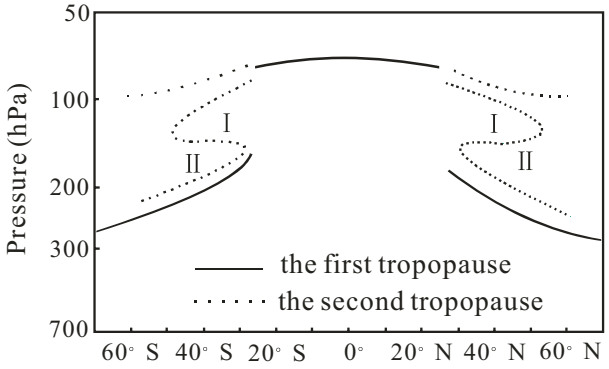

Fig. 4. Schematic diagram of a DT. The air between the first tropopause (thick black line) and second tropopause (thin black line) is separated into type I (tropospheric air) and II (stratospheric air).

tories to find out their origin. Thirty-day backward trajectories are started on 31 December, 31 January, and 28 February for each year between 2003 and 2012.

Figure 5 shows the composite fraction and geographical locations of the air parcels crossing the pressure levels of 700 hPa, 500 hPa, 300 hPa, 200 hPa and 100 hPa before entering DTs in winter (DJF). At or below the pressure level of 300 hPa, for the Northern Hemisphere, air is transported from the western Pacific and central Pacific region in the tropics and the Amazon basin between the equator and the Tropic of Capricorn; while for the Southern Hemisphere, air is mainly transported from the western Pacific region. At the pressure levels of 200 hPa and 100 hPa, where the DTs exist, air may be transported into the DTs from both higher and lower latitudes. As shown in Fig. 6, the source regions in summer for the Southern Hemisphere are dominated by the western tropical Pacific, the Himalayan plateau and Indian subcontinent, and a thin equatorial source corresponding to the Intertropical Convergence Zone (ITCZ). For the Northern Hemisphere, the eastern tropical Pacific between the equator and the Tropic of Cancer is also a dominant region.

For both hemispheres, air initialized within DTs comes from regions of strong convection and steep orography, and paths for the trajectories from the troposphere are relatively concentrated. Only a fraction of air parcels have existed at 300 hPa and even lower levels in the troposphere before entering into DTs, and the fraction grows as pressure decreases. For the Southern Hemisphere, the fraction of trajectories is smaller and the horizontal range of the paths is narrower than those for the Northern Hemisphere on each pressure surface.

The distribution and strength in Fig. 5 to Fig. 6 show a strong seasonality following the seasonal shift of the strong upwelling regions in the tropics and subtropics, as depicted by the long-term mean outgoing longwave radiation (OLR) in Fig. 7. The OLR data are from the National Oceanic and Atmospheric Administration (NOAA) Interpolated OLR product.

Although the source regions are constrained, the pathways of trajectories were not found to enter into DTs directly in the convective areas. As well-established research states, only a small fraction of convective systems can overshoot the tropopause and inject air into the stratosphere, and

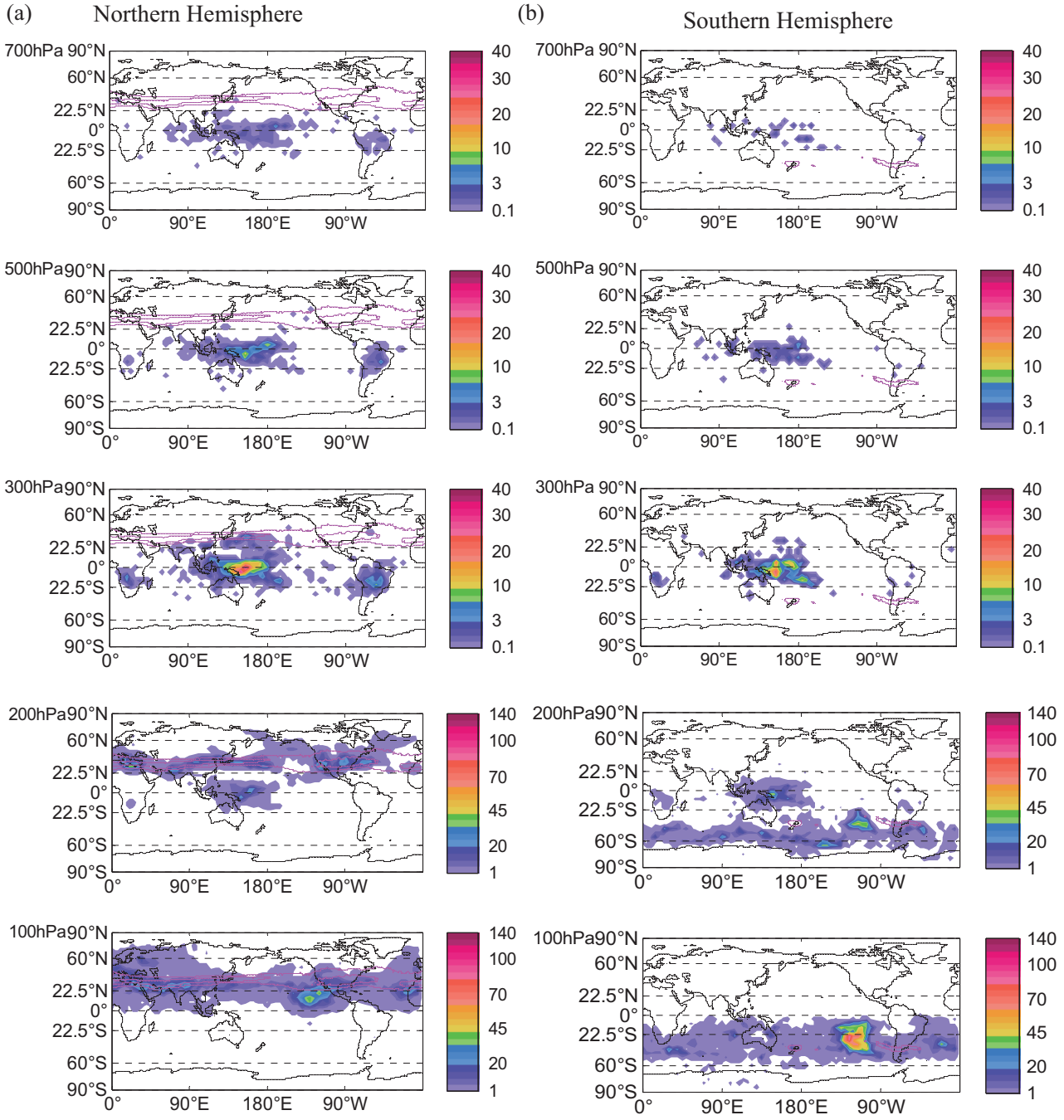

Fig. 5. Proportion and origin of the air sandwiched within DTs on pressure levels of 700, 500, 300, 200 and 100 hPa in winter (DJF; 30-day backward trajectories are started on 31 December, 31 January and 28 February of each year from 2003 to 2012). Figures in column (a) are for DTs in the Northern Hemisphere and figures in column (b) are for DTs in the Southern Hemisphere. Results are binned every 5° of longitude and latitude. Unit: 0.01%. The DT occurrence frequency of 20% (and 40% in the Northern Hemisphere) is shown with magenta contours to denote the horizontal destination of the air parcels. Note the color scheme for the pressure levels of 200 and 100 hPa is different from other pressure levels.

the majority of air parcels rising from the troposphere have to travel several thousand kilometers before entering the upper-troposphere–lower-stratosphere (UTLS) region (Fueglistaler et al., 2004), including DTs.

Figure 8 gives the total fraction of air parcels that have existed at specified pressure levels before entering DTs for four scenarios. The black and red solid lines denote the Northern Hemisphere in winter (DJF) and summer (JJA), respectively, and the black and red dashed lines are for the Southern Hemisphere. As seen in this figure, no more than 15% of the air between DTs has existed at 300 hPa or even lower in the troposphere. From 300 hPa up to about 150 hPa, the fraction

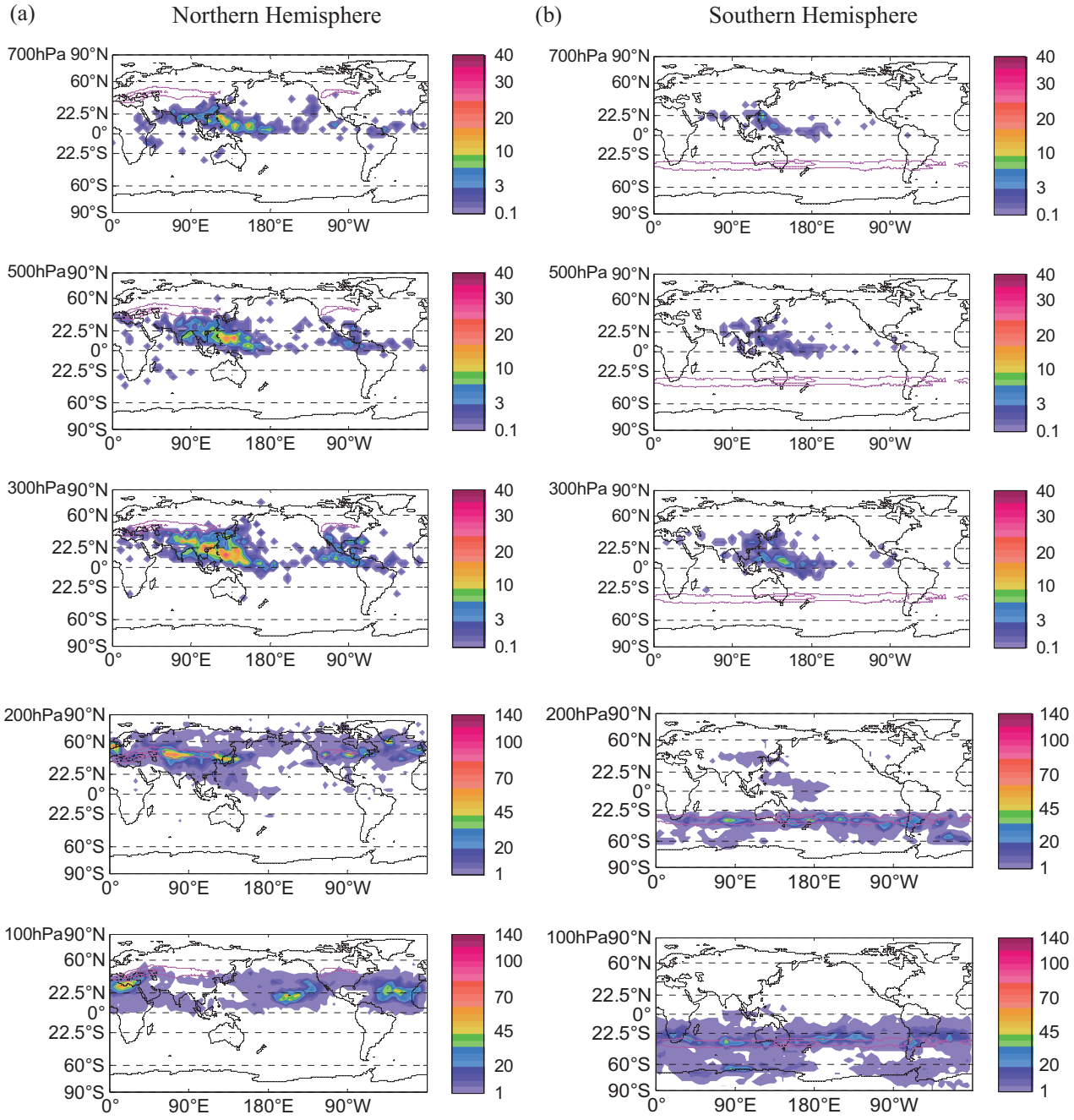

Fig. 6. As in Fig. 5 but in summer (JJA; 30-day backward trajectories are started on 30 June, 31 July and 31 August of each year from 2003 to 2012). The DT occurrence frequency of 20% (and 40% in the Southern Hemisphere) is shown with magenta contours to denote the horizontal destination of the air parcels.

for the four scenarios increases and peaks at about 150 hPa, which is not unexpected because this is the altitude where air between a DT is mostly likely to reside. From 150 hPa to 100 hPa, the fraction begins to decrease. For the Northern Hemisphere, the fraction in summer is much larger than that in winter; for the Southern Hemisphere, the difference between the fraction in winter and summer is very small, except that between 400 hPa and 200 hPa, the fraction in winter exceeds that in summer. Overall, in the summer hemisphere, a larger fraction of air within DTs is transported from below 300 hPa, but it should be noted that there are almost twice as many DTs in winter as in summer.

5. Discussion

The climatological features in section 3 are all based on DTs derived from ERA-Interim data using the modified WMO (1957) criteria stated in section 2. Similar modification has been applied in previous studies when defining the second tropopauses of DTs with reanalysis data (e.g., Randel

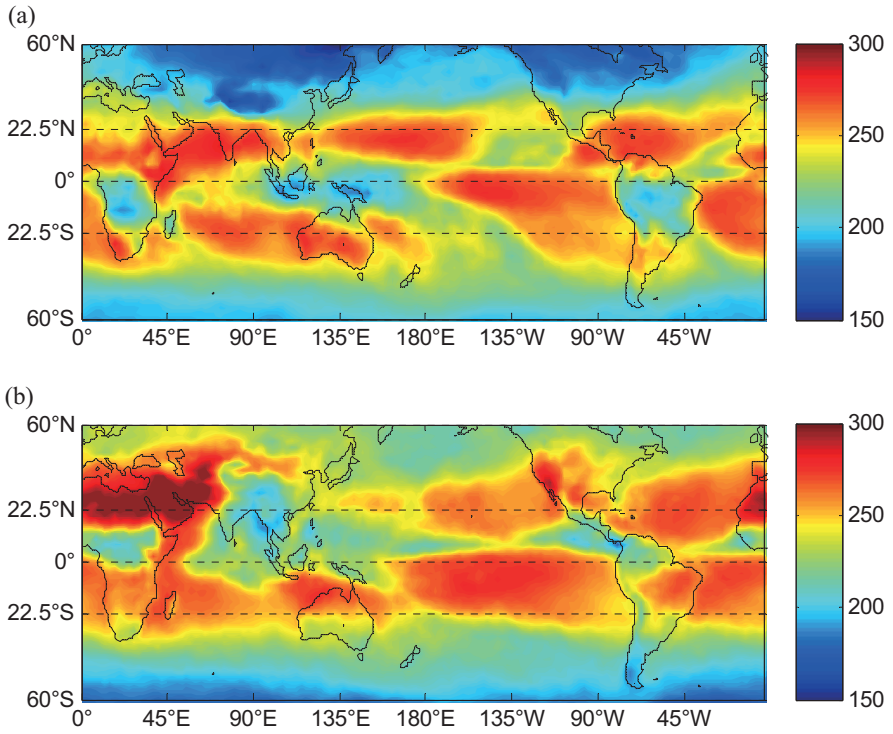

Fig. 7. Long-term (1974–2013) seasonal mean of the OLR for (a) winter (DJF) and (b) summer (JJA); units: W m^{-2}.

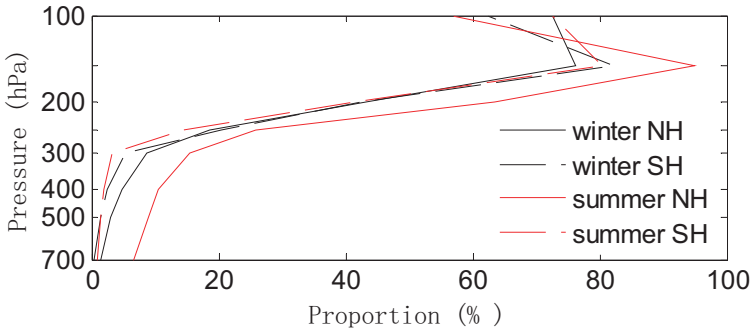

Fig. 8. Proportion of air that has existed at each pressure level before entering into DTs. The black and red solid lines denote the Northern Hemisphere in winter (DJF) and summer (JJA), respectively, and the black and red dashed lines are for the Southern Hemisphere in winter (DJF) and summer (JJA).

et al., 2007; and Castanheira and Gimeno, 2011). To verify the accuracy of the modification, the frequencies of occurrence were also calculated using the temperature profiles from GPS radio occultation measurements from the Constellation Observing System for Meteorology, Ionosphere, and Climate (COSMIC) mission (Anthes et al., 2008) between December 2006 and August 2012, as shown in Fig. 9. The wet temperature profiles were downloaded from the COSMIC Data Analysis and Archive Center of the University Corporation for Atmospheric Research. The precision of each radio occultation (RO) profile could reach $\sim 0.05^{\circ}$C in the UTLS region (Anthes et al., 2008) and the vertical resolution is 0.1 km.

Comparing with Fig. 9, the frequencies in Fig. 2 show similarities both in horizontal range and magnitude, suggesting it should be reasonable to use the reduced (2.5 K km^{-1}) constraint when using ERA40 data for identifying DT occurrences.

Derivation of DT statistics from reanalysis data using the standard WMO (1957) criteria gives far fewer occurrences (Randel et al., 2007), and the reason may be two-fold. The WMO (1957) criteria are very sensitive to temperature profiles (Zängl and Hoinka, 2001). The ERA-40 or ERA-Interim data with low vertical resolution probably lose large temperature gradients above the first tropopause (Randel et al., 2007). Also, the accuracy of temperature profiles may have effects

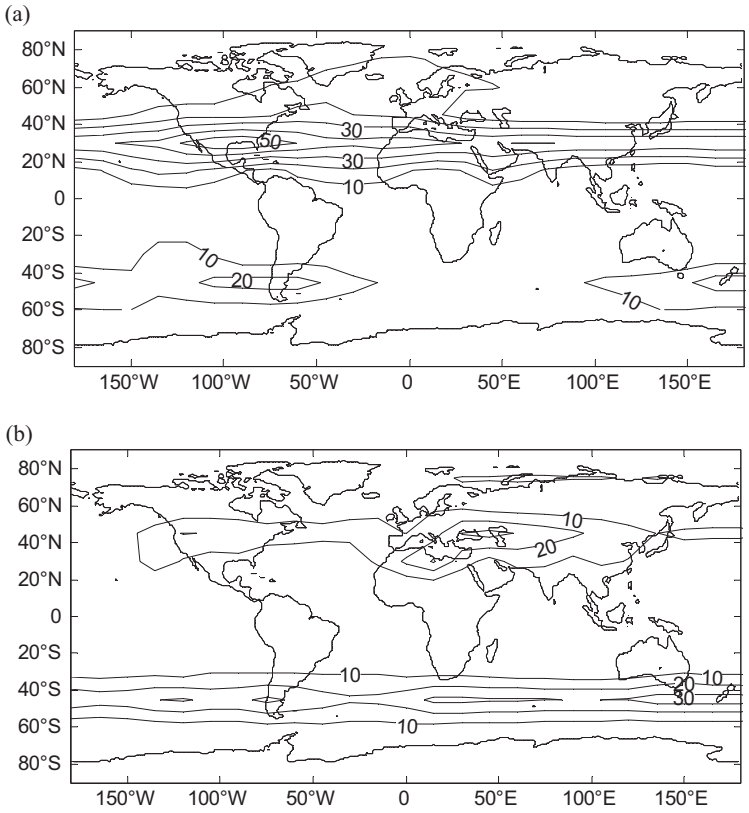

Fig. 9. Climatological frequency of occurrence (%) of DTs derived from COSMIC temperature profiles during 2006–2012, for (a) winter (DJF) and (b) summer (JJA). Contour interval is 10%.

on the frequencies of DTs. As an updated version of ERA-40 data, the ERA-Interim data could produce DT frequencies comparable to RO data by reducing the constraint to 2.5 K km^{-1} (Castanheira and Gimeno, 2011; Castanheira et al., 2012), while the constraint for ERA-40 should be reduced to 2 K km^{-1} to obtain reasonable DT frequencies. Overall, the large DT frequencies in Fig. 2 agree well spatially with previous results from reanalysis or observation data (Schmidt et al., 2006; Añel et al., 2007; Castanheira and Gimeno, 2011; Peevey et al., 2012), albeit there are minor differences in the values that may result from different data and calculating algorithms.

For the results in section 4, there is an important point to be made about the time length of the backward trajectories used to examine the origin of air within DTs. To verify the effectiveness of the 30-day backward trajectories, the calculations were repeated with backward trajectories of 15 days and 60 days. The results (not shown) indicated that the horizontal origin of air within DTs was unaffected by trajectory length changes within the above ranges (15 days, 30 days, and 60 days). The proportion of air in Fig. 5 and Fig. 6 also remained largely unaltered when using 30-day and 60-day backward trajectories; but when using 15-day backward trajectories, the proportion did reduce a little from the 30-day cases. This might be attributable to the fact that the 15-day trajectories may ignore a minority of air transported over a longer period from the troposphere to the extratropical UTLS region (Fueglistaler et al., 2004). So, 30-day trajectories is an appropriate choice to balance the computation cost and transportation time of air parcels.

As stated in section 4, the geophysical location and proportion of the origin of air within DTs vary between seasons. Moreover, they may also vary substantially from year to year. Since the main sources of transport from the lower or middle troposphere to DTs are associated with regions of deep convection, i.e., the western tropical Pacific and Maritime Continent, the Himalayan plateau, and a thin equatorial source corresponding to the ITCZ, any event that may influence these areas would have effects on the air source. For instance, El Niño–Southern Oscillation (ENSO) circulation is one of the most effective factors. ENSO's effects on the strength of tropical upwelling and stratosphere–troposphere exchange have been clearly demonstrated (Scaife et al., 2003; Zeng and Pyle, 2005). Plus, there have been studies on the origin of air in the tropical tropopause layer showing that, in positive phases of ENSO (El Niño years), the source region is shifted towards the eastern Pacific in all seasons, while in negative phases of ENSO (La Niña years) the Himalayas contribute more as a source region of boundary layer air in the Northern Hemisphere summer. To further study the main factors influencing the origin of air in DTs, data over a longer time range are needed.

6. Summary

The 10-year climatological features of midlatitude DT events have been analyzed using ERA-Interim data from 2003 to 2012. The results show that, in the midlatitudes, DTs are permanent or semi-permanent and occur throughout the year. In the Northern Hemisphere winter, high DT frequencies happen between 30°N and 45°N; while in the Southern Hemisphere winter, high DT frequencies are located between 25°S and 45°S. High DT frequency bands move poleward in winter and equatorward in summer, which is consistent with the seasonal movement of the subtropical jet. Based on our results, the second tropopauses of DTs exist at about 100 hPa in the subtropics, and slightly lower in sub-polar regions. The DT thickness, which is defined by the height differences between the first and second tropopause, is smaller in the subtropics and increases with latitude.

A 3-D trajectory-based Lagrangian model was then employed to track the origin of air sandwiched within DTs. The results show that only a fraction (less than 15%) of air sandwiched within DTs originates in the lower or middle troposphere. Additionally, the fraction of air within Northern Hemisphere DTs coming from 300 hPa or even lower in the troposphere is larger in summer (JJA) than in winter (DJF), while this difference is not clearly observed in the Southern Hemisphere. The dominant source regions vary with season following the seasonal shift of strong upwelling regions in the tropics and subtropics, and they are all located over deep convection and steep orography, e.g., the western and central Pacific, the Amazon basin and Himalayan plateau.

Acknowledgements. We thank Dr. Sue Yu LIU for providing the OFFLINE3_diab model and for her helpful suggestions. The ERA-Interim data were obtained from the ECMWF via www.ecmwf.int. The COSMIC data were obtained from the COSMIC Data Analysis and Archive Center via http://cdaac-www.cosmic.ucar.edu/cdaac/index.html. The OLR data were obtained from the NOAA Earth Science Research Laboratory via http://www.esrl.noaa.gov/. This work was supported by the Special Fund for Strategic Pilot Technology of the Chinese Academy of Sciences (Grant No. XDA05040300).

REFERENCES

Añel, J. A., J. C. Antuña, L. de la Torre, R. Nieto, and L. Gimeno, 2007: Global statistics of multiple tropopauses from the IGRA database. *Geophys. Res. Lett.*, **34**(6), L06709, doi: 10.1029/2006GL029224.

Añel, J. A., J. C. Antuña, L. de la Torre, J. M. Castanheira, and L. Gimeno, 2008: Climatological features of global multiple tropopause events. *J. Geophys. Res.*, **113**, D00B08, doi: 10.1029/2007JD009697.

Añel, J. A., L. de la Torre, and L. Gimeno, 2012: On the origin of the air between multiple tropopauses at midlatitudes. *The Scientific World Journal*, **2012**, 191028, doi: 10.1100/2012/191028.

Anthes, R. A., and Coauthors, 2008: The COSMIC/FORMOSAT-3 mission: Early results. *Bull. Amer. Meteor. Soc.*, **89**(3), 313–333, doi: 10.1175/BAMS-89-3-313.

Berthet, G., J. G. Esler, and P. H. Haynes, 2007: A Lagrangian perspective of the tropopause and the ventilation of the lowermost stratosphere. *J. Geophys. Res.*, **112**, D18102, doi: 10.1029/2006JD008295.

Biondi, R., T. Neubert, S. Syndergaard, and J. Nielsen, 2011: Measurements of the upper troposphere and lower stratosphere during tropical cyclones using the GPS radio occultation technique. *Adv. Space Res.*, **47**(2), 348–355.

Bracci, A., and Coauthors, 2012: Transport of stratospheric air masses to the Nepal climate observatory-pyramid (Himalaya; 5079 m MSL): A synoptic-scale investigation. *J. Appl. Meteorol. Clim.*, **51**(8), 1489–1507, doi: 10.1175/JAMC-D-11-0154.1.

Castanheira, J. M., and L. Gimeno, 2011: Association of double tropopause events with baroclinic waves. *J. Geophys. Res.*, **116**, D19113, doi: 10.1029/2011JD016163.

Castanheira, J. M., T. R. Peevey, C. A. F. Marques, and M. A. Olsen, 2012: Relationships among Brewer-Dobson circulation, double tropopauses, ozone and stratospheric water vapour. *Atmos. Chem. Phys*., **12**, 12 391–12 421.

Dee, D. P., and Coauthors, 2011: The ERA-Interim reanalysis: configuration and performance of the data assimilation system. *Quart. J. Roy. Meteor. Soc.* **137**, 553–597. doi: 10.1002/qj.828.

Fueglistaler, S., H. Wernli, and T. Peter, 2004: Tropical troposphere-to-stratosphere transport inferred from trajectory calculations. *J. Geophys. Res.*, **109**(D3), D03108, doi: 10.1029/2003JD004069.

Holton, J. R., 2004: *An Introduction to Dynamic Meteorology*. 4th ed., Burlington, San Diego and London, Academic Press, 535 pp.

Homeyer, C. R., K. P. Bowman, L. L. Pan, E. L. Atlas, R.-S. Gao, and T. L. Campos, 2011: Dynamical and chemical characteristics of tropospheric intrusions observed during START08. *J. Geophys. Res.*, **116**, D06111, doi: 10.1029/2010JD015098.

Horinouchi, T., F. Sassi, and B. A. Boville, 2000: Synoptic-scale Rossby waves and the geographic distribution of lateral transport routes between the tropics and the extratropics in the lower stratosphere. *J. Geophys. Res.*, **105**(D21), 26 579–26 592, doi: 10.1029/2000JD900281.

Lamarque, J.-F., and P. G. Hess, 1994: Cross-tropopause mass exchange and potential vorticity budget in a simulated tropopause folding. *J. Atmos. Sci.*, **51**(15), 2246–2269, doi: 10.1175/1520-0469051.

Manney, G. L., M. I. Hegglin, W. H. Daffer, M. J. Schwartz, M. L. Santee, and S. Pawson, 2014: Climatology of upper tropospheric-lower stratospheric (UTLS) jets and tropopauses in MERRA. *J. Climate*, **27**(9), 3248–3271.

McIntyre, M. E., and T. N. Palmer, 1983: Breaking planetary waves in the stratosphere. *Nature*, **305**, 593–600, doi: 10.1038/305593a0.

Methven, J., 1997: Offline trajectories: Calculation and accuracy UGAMP Tech. Rep. 44, Dep. of Meteorol., Univ. of Reading, Reading, U. K., 18 pp.

Newman, P. A., and M. R. Schoeberl, 1995: A reinterpretation of the data from the NASA Stratosphere-Troposphere exchange project. *Geophys. Res. Lett.*, **22**(18), 2501–2504, doi: 10.1029/95GL02220.

Olsen, M. A., A. R. Douglass, P. A. Newman, J. C. Gille, B. Nardi, V. A. Yudin, D. E. Kinnison, and R. Khosravi, 2008: HIRDLS observations and simulation of a lower stratospheric intrusion

of tropical air to high latitudes. *Geophys. Res. Lett.*, **35**(21), L21813. doi: 10.1029/2008GL035514.

Olsen, M. A., A. R. Douglass, M. R. Schoeberl, J. M. Rodriquez, and Y. Yoshida, 2010: Interannual variability of ozone in the winter lower stratosphere and the relationship to lamina and irreversible transport. *J. Geophys. Res.*, **115**, D15305, doi: 10.1029/2009JD013004

Pan, L. L., and Coauthors, 2009: Tropospheric intrusions associated with the secondary tropopause. *J. Geophys. Res.*, **114**, D10302, doi: 10.1029/2008JD011374.

Pan, L. L., and Coauthors, 2010: The stratosphere-troposphere analyses of regional transport 2008 experiment. *Bull. Amer. Meteor. Soc.*, **91**(3), 327–342, doi: 10.1175/2009BAMS 2865.1.

Pan, L. L., and L. A. Munchak, 2011: Relationship of cloud top to the tropopause and jet structure from CALIPSO data. *J. Geophys. Res.*, **116**(D12), D12201, doi: 10.1029/2010JD015462.

Peevey, T. R., J. C. Gille, C. E. Randall, and A. Kunz, 2012: Investigation of double tropopause spatial and temporal global variability utilizing High Resolution Dynamics Limb Sounder temperature observations. *J. Geophys. Res.*, **117**, D01105, doi: 10.1029/2011JD016443.

Peevey, T. R., J. C. Gille, C. R. Homeyer, and G. L. Manney, 2014: The double tropopause and its dynamical relationship to the tropopause inversion layer in storm track regions. *J. Geophys. Res.*, **119**(17), 10 194–10 212.

Ploeger, F., P. Konopka, G. Günther, J.-U. Grooß, and R. Müller, 2010: Impact of the vertical velocity scheme on modeling transport in the tropical tropopause layer. *J. Geophys. Res.*, **115**, D03301, doi: 10.1029/2009jd012023.

Ploeger, F., and Coauthors, 2011: Insight from ozone and water vapour on transport in the tropical tropopause layer (TTL). *Atmos. Chem. Phys.*, **11**, 407–419, doi: 10.5194/acp-11-407-2011.

Randel, W. J., D. J. Seidel, and L. L. Pan, 2007: Observational characteristics of double tropopauses. *J. Geophys. Res.*, **112**(D7), D07309, doi: 10.1029/2006jd007904.

Scaife, A. A., N. Butchart, D. R. Jackson, and R. Swinbank, 2003: Can changes in ENSO activity help to explain increasing stratospheric water vapor? *Geophys. Res. Lett.*, **30**, doi: 10.1029/2003GL017591.

Schmidt, T., G. Beyerle, S. Heise, J. Wickert, and M. Rothacher, 2006: A climatology of multiple tropopauses derived from GPS radio occultations with CHAMP and SAC-C. *Geophys. Res. Lett.*, **33**(4), L04808, doi: 10.1029/2005GL024600.

Simmons, S. M., S. M. Uppala, D. Dee, and S. Kobayashi, 2006: ERA-interim: New ECMWF reanalysis products from 1989 onward. *ECMWF Newsletter*, **110**, 25–35.

Skerlak, B., M. Sprenger, and H. Wernli, 2013: A global climatology of stratosphere-troposphere exchange using the ERA-interim dataset from 1979 to 2011. *Atmos. Chem. Phys.*, **13**(5), 11537–11595, doi: 10.5194/acpd-13-11537-2013.

Sprenger, M., M. Croci-Maspoli, and H. Wernli, 2003: Tropopause folds and cross-tropopause exchange: A global investigation based upon ECMWF analyses for the time period March 2000 to February 2001. *J. Geophys. Res.*, **108**(D12), 8518, doi: 10.1029/2002JD002587.

Stohl, A., 1998: Computation, accuracy and applications of trajectories-A review and bibliography. *Atmos. Environ.*, **32**(6), 947–966, doi: 1016/s1352-2310(97)00457-3.

Thuburn, J., and G. C. Craig, 2002: On the temperature structure of the tropical substratosphere. *J. Geophys. Res.*, **107**(D2), ACL 10-1–ACL 10-10, doi: 10.1029/2001jd000448.

Vaughan, G., and C. Timmis, 1998: Transport of near-tropopause air into the lower midlatitude stratosphere. *Quart. J. Roy. Meteor. Soc.*, **124**(549), 1559–1578, doi: 10.1256/smsqj.54909.

Vogel, B., and Coauthors, 2011: Transport pathways and signatures of mixing in the extratropical tropopause region derived from Lagrangian model simulations. *J. Geophys. Res.*, **116**, D05306, doi: 10.1029/2010jd014876.

Wang, S., and L. M. Polvani, 2011: Double tropopause formation in idealized baroclinic life cycles: The key role of an initial tropopause inversion layer. *J. Geophys. Res.*, **116**, D05108, doi: 10.1029/2010jd015118.

Waugh, D. W., and L. M. Polvani, 2000: Climatology of intrusions into the tropical upper troposphere. *Geophys. Res. Lett.*, **27**(23), 3857–3860, doi: 10.1029/2000gl012250.

WMO, 1957: Meteorology—A three-dimensional science: Second session of the Commission for Aerology. *WMO Bulletin*, **4**, 134–138.

Yamanaka, M. D., 1992: Formation of multiple tropopause and stratospheric inertio-gravity waves. *Advances in Space Research*, **12**(10), 181–190.

Yamanaka, M. D., S. Ogino, S. Kondo, T. Shimomai, S. Fukao, Y. Shibagaki, Y. Maekawa, and I. Takayabu, 1996: Inertio-gravity waves and subtropical multiple tropopauses: Vertical wavenumber spectra of wind and temperature observed by the MU radar, radiosondes and operational rawinsonde network. *J. Atmos. Terr. Phys.*, **58**(6), 785–805.

Zängl, G., and K. P. Hoinka: 2001: The tropopause in the polar regions. *J. Climate*, 14(14), 3117–3139.

Zeng, G., and J. A. Pyle, 2005: Influence of El Niño Southern Oscillation on stratosphere/troposphere exchange and the global tropospheric ozone budget. *Geophys. Res. Lett.*, **32**, L01814, doi: 10.1029/2004gl021353.